minerals

MDPI

Article

REE Tetrad Effect and Sr-Nd Isotope Systematics of A-Type Pirrit Hills Granite from West Antarctica

Hyo Min Lee [1], Seung-Gu Lee [2,*], Hyeoncheol Kim [2], Jong Ik Lee [3] and Mi Jung Lee [3]

[1] Geoscience Platform Division, Korea Institute of Geoscience and Mineral Resources, 124 Gwahak-ro, Yuseong-gu, Daejeon 34132, Korea; hmlee@kigam.re.kr
[2] Geology Division, Korea Institute of Geoscience and Mineral Resources, 124 Gwahak-ro, Yuseong-gu, Daejeon 34132, Korea; hckim@kigam.re.kr
[3] Division of Polar Earth-System Sciences, Korea Polar Research Institute, 26 Songdomirae-ro, Yeonsu-gu, Incheon 21990, Korea; jilee@kopri.re.kr (J.I.L.); mjlee@kopri.re.kr (M.J.L.)
* Correspondence: sgl@kigam.re.kr; Tel.: +82-42-868-3376

Abstract: The Pirrit Hills are located in the Ellsworth–Whitmore Mountains of West Antarctica. The Pirrit Hills granite exhibits significant negative Eu anomalies (Eu/Eu* = 0.01~0.25) and a REE tetrad effect indicating intensive magmatic differentiation. Whole-rock Rb-Sr and Sm-Nd geochronologic analysis of the Pirrit Hills granite gave respective ages of 172.8 ± 2.4 Ma with initial $^{87}Sr/^{86}Sr$ = 0.7065 ± 0.0087 Ma and 169 ± 12 Ma with initial $^{144}Nd/^{143}Nd$ = 0.512207 ± 0.000017. The isotopic ratio data indicate that the Pirrit Hills granite formed by the remelting of Mesoproterozoic mantle-derived crustal materials. Both chondrite-normalized REE patterns and Sr-Nd isotopic data indicate that the Pirrit Hills granite has geochemical features of chondrite-normalized REE patterns indicating that REE tetrad effects and negative Eu anomalies in the highly fractionated granites were produced from magmatic differentiation under the magmatic-hydrothermal transition system.

Keywords: A-type granite; Pirrit Hills; West Antarctica; REE tetrad effect; Rb-Sr; Sm-Nd isotopes

check for updates

Citation: Lee, H.M.; Lee, S.-G.; Kim, H.; Lee, J.I.; Lee, M.J. REE Tetrad Effect and Sr-Nd Isotope Systematics of A-Type Pirrit Hills Granite from West Antarctica. *Minerals* **2021**, *11*, 792. https://doi.org/10.3390/min11080792

Academic Editors: Lucie Mathieu, Michel Jébrak and Nadia Mohammadi

Received: 6 July 2021
Accepted: 20 July 2021
Published: 22 July 2021

Publisher's Note: MDPI stays neutral with regard to jurisdictional claims in published maps and institutional affiliations.

Copyright: © 2021 by the authors. Licensee MDPI, Basel, Switzerland. This article is an open access article distributed under the terms and conditions of the Creative Commons Attribution (CC BY) license (https://creativecommons.org/licenses/by/4.0/).

1. Introduction

Rare earth element (REE) signatures in whole-rock samples can help constrain igneous petrogenetic processes. Magmatic fractionation causes systematic fractionation in chondrite-normalized REE patterns of the granitic rocks due to the generally similar chemical behavior and continuous decrease in the ionic radii, i.e., lanthanide contraction of the lanthanide series [1–17].

The REE tetrad effect [1] is a specific feature of chondrite-normalized REE patterns, which forms four curved segments with each curve consisting of four REEs (La-Ce-Pr-Nd, Pm-Sm-Eu-Gd, Gd-Tb-Dy-Ho, and Er-Tb-Yb-Lu). Additionally, highly fractionated igneous rocks such as felsic granite and high silica rhyolite frequently exhibit the REE tetrad effect. In order to understand the cause and mechanism of the REE tetrad effect in geological rocks, we need to clarify: (1) what kind of mechanism produces the REE tetrad effect in the geological rocks; (2) when the REE tetrad effect was formed in the geological rocks such as highly fractionated granite; and (3) why the highly fractionated granite with REE tetrad effect has extremely large Eu negative anomaly compared to those without REE tetrad effect.

Since an initial report by Masuda and Akagi [2] on REE tetrad effects in a leucogranite from China, considerable research groups have tried to clarify the formation mechanism of the REE tetrad effect in the granitoids [3–17]. Most research results have mentioned that this specific REE distribution pattern might be formed by modification of the geochemical behavior of REEs in the fluid-rich melt during magmatic-hydrothermal transition [3–13]. Some groups argue that the REE tetrad effect in highly fractionated granites might be derived from mineral fractionation rather than by fluid-melt interaction [14,15]. However,

Lee et al. [16–18] argued that, based on the Rb-Sr, La-Ce, Sm-Nd isotopic system, the REE tetrad patterns were formed by magmatic differentiation rather than hydrothermal alteration. Recently, Shuai et al. [15] also proposed that, based on the modelling using partition coefficients of REEs between minerals and granitic melts, the REE tetrad effect was inherited from residual magmas that have experienced mineral fractionation. Like this, the cause, formation mechanism, and formation stages of the REE tetrad effect are not yet clear and research ongoing.

One of the peculiar geochemical features of highly fractionated granite with REE tetrad effect is an extremely large negative Eu anomaly ($Eu/Eu^* < 0.1$). Irber [4] reported the correlation between degree of Eu anomaly and the REE tetrad effect. Though Shuai et al. [15] proposed that the REE tetrad effect was derived from mineral fractionation based on the modelling using partition coefficients of REEs between minerals and granitic melts, the authors did not mention the order between REE tetrad effect and extremely large Eu negative anomaly. It suggests that we may need to clarify the context of the formation stage between the REE tetrad effect and the Eu anomaly.

In igneous rocks, the negative Eu anomaly is the product of feldspar fractionation related to oxygen fugacity in the magma [19–23]. It means that the order between REE tetrad effect and extremely large Eu negative anomaly may become a key to clarify the origin related to the formation of the REE tetrad effect such as pure magmatic origin or magmatic-hydrothermal transition.

Generally, Sr, Nd, and Pb isotopic data provide the source characters if the magma was not contaminated by country rocks or not mixed with other kind of magma. Additionally, the Sm-Nd isotopic system is less susceptible to alteration and metasomatism whereas the Rb-Sr isotopic system is susceptible to the above reactions. In addition, U-Pb zircon and Sm-Nd whole isochron ages from the granite indicate magmatic ages of source magma. Therefore, agreement among the Rb-Sr, Sm-Nd, and U-Pb isotopic ages from a granite can be interpreted as showing geochemical features related to an evolutionary process of the granitic source magma. However, data including all of the Sr, Nd, and Pb isotopic data for granites with the REE tetrad effect have been reported very rarely because the dating of a whole rock Sm-Nd isotope system is difficult in granitic rocks with young geological ages.

The Jurassic Pirrit Hills granite in Antarctica is highly fractionated, A-type granite, which occurs as a relatively isolated pluton within the Ellsworth–Whitmore Mountains (EWM) block of West Antarctica and offers an interesting example of magmatism associated with large scale continental break-up processes [24,25]. The geochemical characteristics for the Pirrit Hills granite, including major, trace, and REE abundances, have been reported in previously published sources [24–26]. In the previous paper, Lee et al. [25] reported the chondrite-normalized REE patterns showing the apparent flatness of these granites with a U-Pb zircon age of 164.5 $\pm$ 2.3 Ma for this body. However, Miller et al. [27] reported 173 $\pm$ 3 Ma Rb-Sr whole-rock isochron ages for Pirrit Hills samples collected from the EWM. Pankhurst et al. [28] reported highly variable Sm-Nd isotopic data. Though another previous report [25,27] also reported chondrite-normalized REE patterns, their data did not suggest tetrad effects because of the absence of Tb and Tm abundance data. However, we noticed that the Jurassic Pirrit Hills granite has a peculiar REE tetrad effect suggesting that the REE tetrad effects should be formed by an evolutionary process from the source magma.

In this study, we measured Rb-Sr and Sm-Nd isotope systematics to determine the emplacement age of the Jurassic Pirrit Hills granite. Particularly, we re-measured REE and some trace element concentrations of previously reported samples to clarify the formation stage of the REE tetrad effect of the Pirrit Hills granite in Antarctica to reconsider the REE redistribution in the granite magma. Therefore, in this paper, we discuss the meaning of the new Rb-Sr and Sm-Nd isotopic data along with more accurate and precise REE data that permit a more precise geochemical interpretation of the Pirrit Hills granite. The geochemical patterns are specifically interpreted in terms of what they reveal about the magmatic history of West Antarctica.

2. Geological Setting and Petrography

Antarctica is divided into East Antarctica and West Antarctica. West Antarctica consists of five crustal blocks separated by deep crustal rift zones interpreted to have shifted during the Mesozoic break-up of Gondwana [24,29,30]. The Jurassic Pirrit Hills granite occurs as a relatively isolated pluton within the Ellsworth–Whitmore Mountains (EWM) block of West Antarctica. It exhibits highly fractionated, A-type geochemical signatures and offers an interesting example of magmatism associated with large scale continental break-up processes [24,25].

Physiographically, Antarctica consists of the East and West Antarctic regions separated by the Transantarctic Mountains (TAM). A set of five discrete, relatively thin (25–30 km) crustal blocks separated by deep rift zones [29] make up West Antarctica. These include the Antarctic Peninsula block (AP), the Ellsworth–Whitmore Mountains block (EWM), the Haag Nunataks block (HN), the Thurston Island block (TI), and the Marie Byrd Land block (MBL) (Figure 1a).

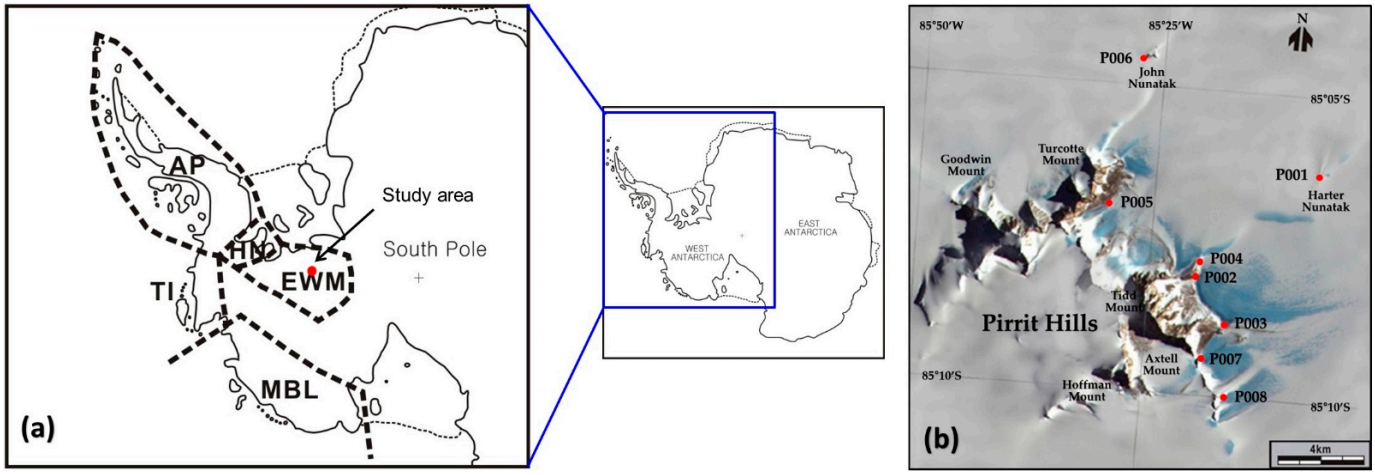


Figure 1. (**a**) Simplified location maps of the study area within West Antarctica. The major crustal blocks include the Antarctic Peninsula (AP), the Ellsworth–Whitmore Mountains (EWM), the Haag Nunataks (HN), Marie Byrd Land (MBL), and Thurston Island (TI) [30]. (**b**) Satellite image of the Pirrit Hills and sampling locations (modified from [25]).

The Pirrit Hills (81°08′ S, 85°25′ W) occur within the EWM, and correspondingly, in the center of West Antarctica. The Pirrit Hills lie among scattered hills and mountains found between the Ellsworth Mountains proper to the north and the Thiel Mountains to the south. These include landforms assigned to the Ellsworth Mountains but also the Pirrit, Nash, and Martin Hills, the Whitmore Mountains, the Pagano Nunatak, the Hart Hills, and landforms assigned to the Thiel Mountains. Within the EWM, igneous bodies intrude deformed Cambrian to Permian strata. The granitic body that makes up the Pirrit Hills is a part of a Jurassic suite [27] further exposed in the Nash Hills, Martin Hills, Whitmore Mountains, and Pagano Nunatak. These post-tectonic plutons intruded deformed Paleozoic strata to form the main exposures of the central EWM block [26,31]. The Pirrit and Nash Hills exposures consist primarily of felsic plutonic rocks surrounded by thermally altered metasedimentary roof pendants [32]. The nature of metamorphic basement or country rock beneath the EWM is uncertain. The Whitmore Mountains form the largest outcrops in the area and exhibit two principal types of granite. The fine-grained leucocratic Linck Nunatak granite intrude these bodies. Pagano Nunatak consists of light gray, massive, medium- to coarse-grained biotite granite intruded by aplite dikes that reach 2 m in width, and which are characterized by sparse muscovite.

The Pirrit Hills granite outcrops are fairly uniform in appearance, consisting mostly of medium- to coarse-grained leucocratic alkali feldspar granite (Figure 2). The Pirrit Hills granite contains partly pegmatite and aplite veins. It mainly consists of quartz, K-feldspar,

plagioclase, biotite, muscovite, and accessory minerals of zircon. Quartz is mostly anhedral and frequently shows undulatory extinction. K-feldspars are mainly perthite with Carlsbad twins and forms micrographic intergrowths with quartz in several samples. Plagioclases are euhedral to subhedral and show albite and locally albite-Carlsbad twinning, some of which are affected by alteration with secondary sericite. Biotites are subhedral with minor alteration to chlorite along grain boundaries and cleavages, and sometimes contain opaque minerals [25].

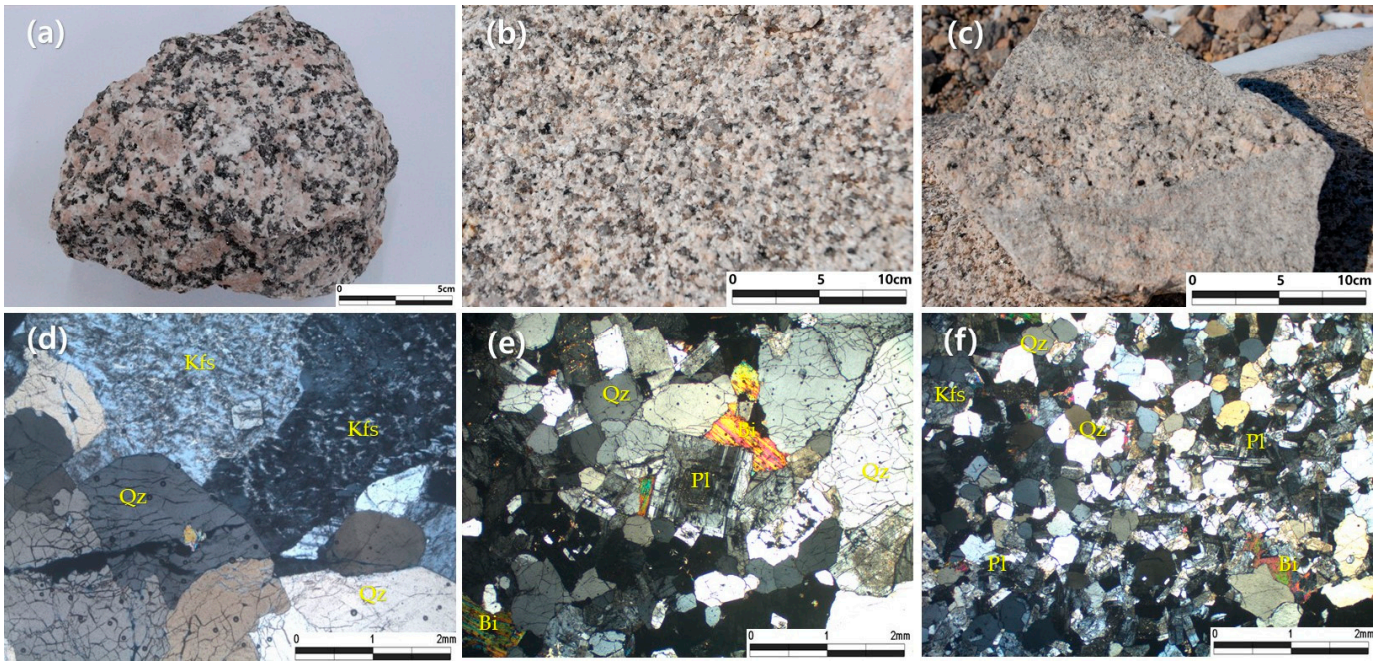


Figure 2. Representative field photographs and photomicrographs (crossed polars) of the Pirrit Hills granite. (**a**) Coarse-grained two mica granite (P008). (**b**) The homogeneous medium-grained granite. (**c**) Aplite vein. (**d**) Coarse-grained two mica granite (P008). (**e**) Medium-grained two mica granite (P005-1). (**f**) Fine-grained two mica granite (P005-2).

3. Analytical Methods

The twelve whole-rock sample powders analyzed for this study were the same as those used by Lee et al. [25]. Commercial ultrapure acids (HF, HNO_3, HCl, Merck Chemical Company, Darmstadt, Germany) were used in all digestion and purification steps. In order to measure background values of various acids, 1 mL of nitric acid, 2 mL of hydrofluoric acid, 0.1 mL of perchloric acid, and 10 mL of hydrochloric acid were mixed, evaporated, and then re-diluted in 2% nitric acid to analyze as blanks. REEs and other trace element abundances were determined by ICP-MS (NexION350, Perkin Elmer, Waltham, MA, USA) at the Korea Institute of Geoscience and Mineral Resources (KIGAM), Daejeon, Korea. Analysis and experimental conditions for rare earth and trace elements (standard reagents and oxide calibration methods, ICP-MS measurement conditions, etc.) are described in Lee et al. [33,34]. The analysis used triple element (In, Re, and Bi) internal standardization corrections for oxide and hydroxide interference. Precision and accuracy of the ICP-MS data were frequently checked using geochemical reference materials, JG2 (granite) and JR2 (rhyolite). Analytical accuracy and precision of REEs fell within 5% (2 σ_m). Chondrite-normalized REE pattern (see Figure 3) for JG2 is smooth and coherent, which agrees well with the published data measured by ICP-AES and ICP-MS [35,36].

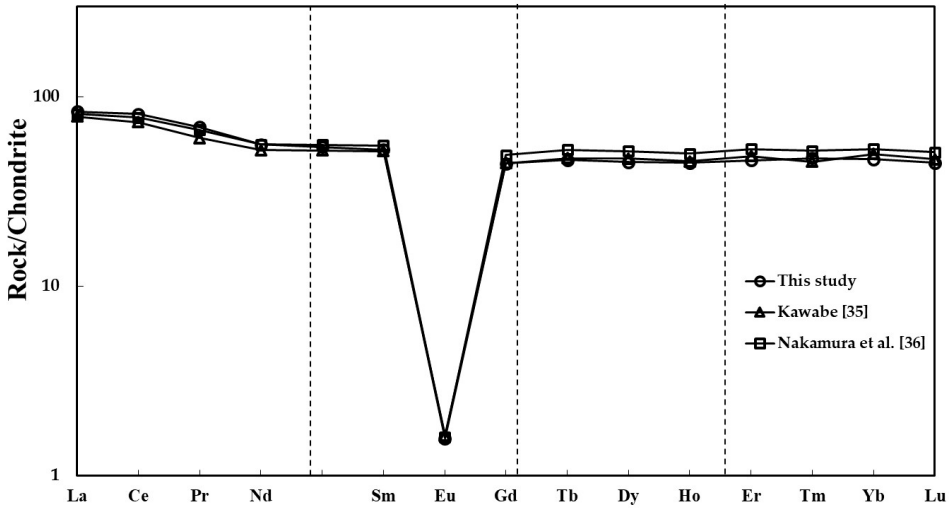


Figure 3. Chondrite-normalized REE pattern of JG2 to compare new data from this study with published values [35,36]. Normalizing chondrite values are taken from McDonough and Sun [37].

Nine samples were subjected to Rb-Sr and Sm-Nd isotopic analysis. Sample preparation for these procedures was conducted in a class 1000 clean room. Approximately 100 mg of each sample was weighed in a 15 mL flat bottom PFA Teflon vial (Minnetonka, MN, USA). Sample powders were then dissolved in concentrated ultrapure HF, HNO_3, and $HClO_4$ for Sr and Nd isotope ratio analysis. After drying the solution, the dried cakes were dissolved in 10 mL of 6 M HCl as a stock solution for isotope dilution for Rb, Sr, Sm, and Nd abundances, and Sr and Nd isotope analysis. Before ion exchange column chromatography, the solutions were checked for visual clarity to ensure total decomposition of the sample. The 10 mL of the stock solution was divided into 2 mL for Rb, Sr, Sm, and Nd abundance determination by isotope dilution method and 8 mL for Sr and Nd natural isotope analysis, respectively. After drying up each aliquoted solution, the cake was dissolved in 0.5 mL of 2.5 M HCl and then centrifuged at 13,000 rpm for 5 min to separate the residual. Rb, Sr, and REE fractions were separated by cation exchange using a DOWEX® (Darmstadt, Germany) 50W-X8, 100~200 mesh column. Sm and Nd fractions were separated from the REE fraction by additional cation column chemistry using a Ln resin (100–150 μm, Eichrom Technologies Inc., Lisle, IL, USA).

Sr and Nd isotopes, including measurements of Sr, Rb, Sm, and Nd abundances, were measured using a TRITON Plus TIMS (thermal ionization mass spectrometer, Thermo Fisher Scientific Inc., Waltham, MA, USA) at KIGAM. The $^{87}Sr/^{86}Sr$ ratios were corrected for mass fractionation by normalizing to $^{88}Sr/^{86}Sr = 8.375209$ using an exponential function. The ^{87}Sr peak was monitored for interference by ^{87}Rb peaks. Sr isotopic ratios were corrected for this interference assuming $^{87}Rb/^{85}Rb = 0.3857$. Replicate analyses of NBS 987 gave $^{87}Sr/^{86}Sr = 0.710267 \pm 0.000003$ (N = 30, 2 σ_m). The total procedural blanks during the Sr isotopic measurements did not exceed 300 pg. The $^{143}Nd/^{144}Nd$ ratios were normalized to $^{146}Nd/^{144}Nd = 0.7219$ using an exponential function. Interferences from ^{144}Sm on ^{144}Nd peaks and from ^{150}Sm on ^{150}Nd peaks were corrected by monitoring ^{147}Sm and assuming $^{147}Sm/^{144}Sm = 4.88273$. However, ^{147}Sm ion beam intensity was low enough to be ignored during measurements. The average value for JNdi-1 was $^{143}Nd/^{144}Nd = 0.512112 \pm 0.000005$ (N = 25, 2 σ_m). The total procedural blanks for Nd isotopic analysis were less than 50 pg. The Rb-Sr and Sm-Nd isochron ages were calculated using the Isoplot/Ex program [38] assuming an uncertainty of 1% on measured Rb/Sr and Sm/Nd ratios and of 0.01% on measured Sr and Nd isotopic ratios.

Zircons of the same amount analyzed by Lee et al. [25] were re-examined with a JSM-IT 200 scanning electron microscope installed at Korea Institute of Geoscience and Mineral Resources. We obtained backscattered electron and cathodoluminescence images of zircons. Most zircon grains, however, did not luminesce.

4. Results

4.1. Chemical Compositon

Table 1 summarizes re-analyzed REE and select trace element data. Figure 4 shows chondrite-normalized REE patterns for the Pirrit Hills granite samples. The REE diagrams are divided into groups exhibiting either LREE enrichment with Eu anomalies (Figure 4a) or LREE depletion (Figure 4b). Tetrad effects also appear. Irber [4] and Monecke et al. [7,8] described methods used here for estimating the size of tetrad effects in rock and mineral samples ($TE_{1,3}$ or T_i in Table 2). Samples with values of $TE_{1,3} > 1.1$ or $T_i > 0.1$ represent convex or concave normalized patterns. The Pirrit Hills granite gives respective T_1, T_3, and T_4 ranges of 0.04 to 0.16, 0.05 to 0.18, and 0.05 to 0.12.

Table 1. Trace and REE concentrations (ppm) for Pirrit Hills granite samples.

Sample	A Group				B Group								Reference	
No.	P004	P006	P007-1	P008	P001	P002	P003-1	P003-2	P005-1	P005-2	P005-3	P007-2	JG2	JR2
Ga	18.62	18.34	18.26	16.49	23.38	19.79	25.00	26.17	20.84	25.89	22.97	22.71	17.82	16.94
Rb	449.23	427.95	435.18	358.92	507.52	514.93	660.85	692.85	669.83	653.47	799.81	511.05	292.82	290.98
Sr	38.31	37.42	38.51	38.99	12.40	16.50	6.15	8.98	10.14	10.93	5.86	7.23	19.50	9.99
Y	67.43	75.08	57.07	27.00	183.86	60.83	36.31	248.73	57.02	60.92	32.78	85.22	79.74	42.96
Zr	100.43	99.56	58.25	47.78	144.43	65.23	41.53	68.47	63.60	44.49	7.97	49.58	112.16	118.94
Nb	41.52	45.94	35.10	35.74	47.47	29.24	32.92	30.19	29.53	59.29	18.20	47.98	21.15	21.52
Ba	116.95	68.22	63.12	80.86	7.34	14.88	3.03	1.51	8.03	2.97	3.89	1.95	56.92	27.12
La	25.31	22.78	17.10	16.89	16.16	10.19	6.41	12.58	5.82	7.87	7.11	6.74	20.04	13.91
Ce	59.27	45.83	38.48	37.72	40.93	22.94	17.19	28.11	15.75	19.85	14.24	16.78	49.82	37.60
Pr	7.36	6.59	5.02	4.59	5.75	3.20	1.98	5.01	2.12	2.80	2.32	2.37	6.34	4.48
Nd	27.97	25.67	19.81	17.30	24.21	13.06	7.73	23.16	9.07	11.56	10.38	9.81	25.62	17.83
Sm	8.30	8.06	6.56	4.77	9.89	5.10	3.40	13.44	4.27	5.86	4.72	4.86	7.77	4.95
Eu	0.40	0.41	0.36	0.39	0.15	0.16	0.03	0.04	0.10	0.04	0.05	0.05	0.09	0.09
Gd	8.72	9.40	7.48	4.85	13.18	6.08	3.77	19.56	5.22	6.64	4.73	6.44	8.89	5.35
Tb	1.69	1.92	1.51	0.90	2.96	1.29	0.79	4.30	1.18	1.52	0.83	1.47	1.66	0.97
Dy	11.46	13.38	10.33	5.86	21.72	9.06	5.37	30.38	8.64	10.66	4.93	10.75	11.28	6.46
Ho	2.43	2.87	2.16	1.19	4.78	1.93	1.07	6.42	1.86	2.15	0.94	2.33	2.42	1.39
Er	7.54	8.83	6.68	3.58	16.07	6.38	3.64	21.19	6.48	7.50	3.04	7.82	7.53	4.46
Tm	1.19	1.33	1.02	0.55	2.78	1.09	0.72	3.75	1.22	1.44	0.53	1.38	1.17	0.73
Yb	7.58	8.15	6.42	3.51	19.29	7.76	5.87	27.53	9.17	11.23	3.98	9.98	7.59	5.13
Lu	1.05	1.10	0.88	0.47	2.93	1.19	0.93	4.27	1.46	1.75	0.63	1.55	1.11	0.79
Hf	4.71	4.40	2.72	2.01	8.36	4.04	4.55	6.02	5.12	4.81	0.92	4.18	5.04	6.40
Ta	3.62	2.23	8.24	6.59	5.27	4.77	16.77	19.12	15.16	25.92	12.81	33.48	8.14	4.80
Th	33.24	35.13	19.41	20.18	43.10	16.93	9.97	19.81	22.37	16.40	2.39	18.76	35.00	33.69
U	9.91	19.76	7.00	6.66	20.01	14.63	10.15	9.27	4.33	9.18	7.71	30.97	10.00	10.48

Table 2. Calculated tetrad effect and geochemical parameters for Pirrit Hills granite samples.

Sample	A Group				B Group							
No.	P004	P006	P007-1	P008	P001	P002	P003-1	P003-2	P005-1	P005-2	P005-3	P007-2
T_1 [a]	0.08	0.06	0.04	0.06	0.07	0.04	0.16	0.09	0.10	0.08	0.11	0.07
T_3 [a]	0.06	0.08	0.09	0.05	0.12	0.11	0.14	0.13	0.13	0.18	0.06	0.13
T_4 [a]	0.06	0.05	0.05	0.07	0.06	0.05	0.12	0.07	0.08	0.11	0.06	0.06
TE_1 [b]	1.08	0.99	1.04	1.06	1.07	1.02	1.14	0.96	1.10	1.08	0.92	1.07
TE_3 [b]	1.06	1.10	1.10	1.04	1.17	1.13	1.15	1.16	1.18	1.21	1.01	1.19
$TE_{1,3}$ [b]	1.07	1.04	1.07	1.05	1.12	1.08	1.14	1.06	1.14	1.14	0.96	1.13

Table 2. *Cont.*

Sample No.	A Group				B Group							
	P004	**P006**	**P007-1**	**P008**	**P001**	**P002**	**P003-1**	**P003-2**	**P005-1**	**P005-2**	**P005-3**	**P007-2**
La/Nb	0.61	0.50	0.49	0.47	0.34	0.35	0.19	0.42	0.20	0.13	0.39	0.14
Rb/Sr	11.73	11.44	11.30	9.21	40.94	31.21	107.52	77.17	66.07	59.79	136.40	70.72
Zr/Hf	21.34	22.65	21.39	23.72	17.27	16.15	9.12	11.37	12.41	9.25	8.62	11.87
Nb/Ta	11.48	20.61	4.26	5.43	9.01	6.13	1.96	1.58	1.95	2.29	1.42	1.43
Sr/Ba	0.33	0.55	0.61	0.48	1.69	1.11	2.03	5.94	1.26	3.68	1.51	3.70
Y/Ho	27.80	26.13	26.45	22.64	38.45	31.59	34.05	38.75	30.59	28.29	35.02	36.55
Eu/Eu* [c]	0.14	0.14	0.16	0.25	0.04	0.09	0.03	0.01	0.06	0.02	0.03	0.03
CIA [d]	50.40	50.51	50.84	50.68	50.55	50.43	51.54	50.74	51.26	51.56	51.05	51.49

[a] $T_1 = (1/2 \times ([(Ce)_{CN}/\{(La)_{CN}{}^{2/3} \times (Nd)_{CN}{}^{1/3}\} - 1]^2 - [(Pr)_{CN}/\{(La)_{CN}{}^{1/3} \times (Nd)_{CN}{}^{2/3}\} - 1]^2))^{1/2}$; $T_3 = (1/2 \times ([(Tb)_{CN}/\{(Gd)_{CN}{}^{2/3} \times (Ho)_{CN}{}^{1/3}\} - 1]^2 - [(Dy)_{CN}/\{(Gd)_{CN}{}^{1/3} \times (Ho)_{CN}{}^{2/3}\} - 1]^2))^{1/2}$; $T_4 = (1/2 \times ([(Tm)_{CN}/\{(Er)_{CN}{}^{2/3} \times (Lu)_{CN}{}^{1/3}\} - 1]^2 - [(Yb)_{CN}/\{(Er)_{CN}{}^{1/3} \times (Lu)_{CN}{}^{2/3}\} - 1]^2))^{1/2}$ [7]. [b] $TE_1 = [(Ce)_N/(Ce^*)_N \times (Pr)_N/(Pr^*)_N]^{1/2}$, $TE_3 = [(Tb)_N/(Tb^*)_N \times (Dy)_N/(Dy^*)_N]^{1/2}$, $TE_{1,3} = (TE_1 \times TE_3)^{1/2}$ [4]. [c] $Eu/Eu^* = Eu_N/(Sm_N \times Gd_N)^{1/2}$. [d] $CIA = [Al_2O_3/(Al_2O_3 + CaO^* + Na_2O + K_2O)] \times 100$ using molecular proportions where in CaO* is the amount of CaO incorporated in the silicate fraction of the rock [39].

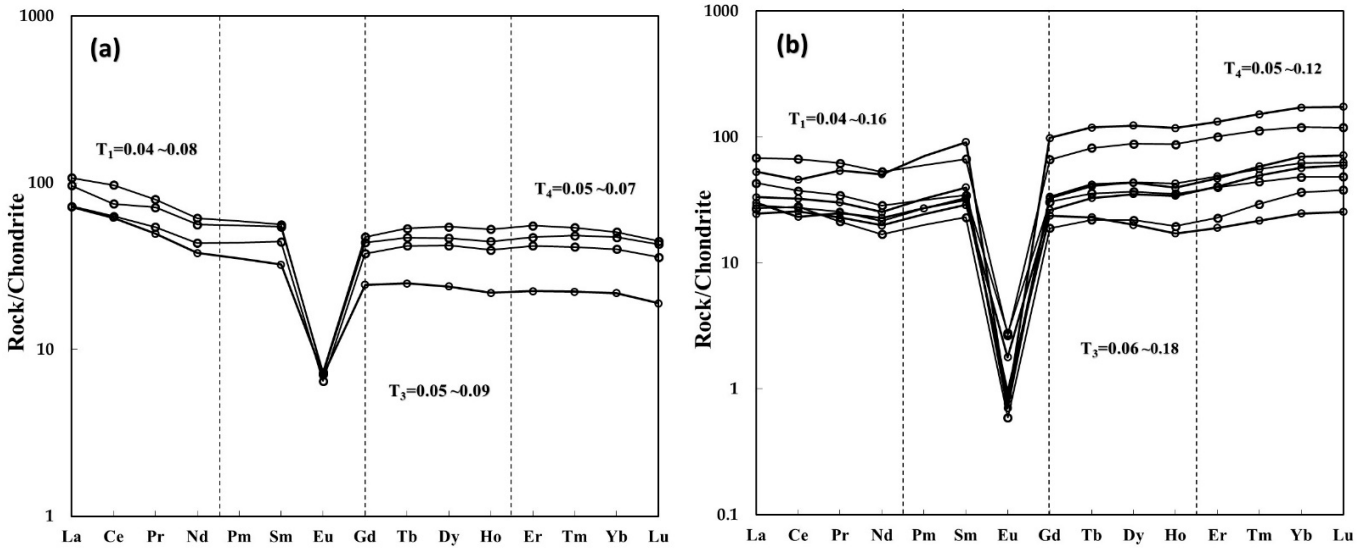


Figure 4. Chondrite [37]-normalized REE distributions for (**a**) A group; Eu/Eu* > 0.1 and (**b**) B group; Eu/Eu* < 0.1 among Pirrit Hills granite samples. The values of T_1, T_3, and T_4 were calculated following equations given in Monecke et al. [7].

4.2. Rb-Sr and Sm-Nd Isotope Systematics

Table 3 lists the whole-rock Rb-Sr and Sm-Nd isotopic compositions for the Pirrit Hills granite samples. Samples analyzed gave $^{87}Sr/^{86}Sr$ ratios of 0.778773 to 2.060016 (2 σ SE) and $^{143}Nd/^{144}Nd$ ratios of 0.512372 to 0.512579 (2 σ SE). Additionally, then, the Rb-Sr whole rock age, including the data reported by Millar and Pankhurst [27], yield 172.8 ± 2.4 Ma (Figure 5a) with $(^{87}Sr/^{86}Sr)_i = 0.7065 \pm 0.0087$, which is almost the same as the of 173 ± 3 Ma by Millar and Pankhurst [27]. The whole-rock Sm-Nd data gave an isochron age of 169 ± 12 Ma with $(^{143}Nd/^{143}Nd)_i = 0.512207 \pm 0.000017$ (Figure 5b) and $\varepsilon_{Nd}(t) = -4.16$.

Table 3. Whole-rock concentrations and Rb-Sr and Sm-Nd isotopic parameters of Pirrit Hills granite samples.

Sample No.	Rb (ppm)	Sr (ppm)	$^{87}Rb/^{86}Sr$	$^{87}Sr/^{86}Sr$ [a]	± 2 σ	$^{87}Sr/^{86}Sr_i$ (172.8 Ma)
P001	487.04	7.66	192.39	1.177538	0.000014	0.704879
P002	505.97	13.99	107.42	0.977485	0.000011	0.713578
P003-1	711.29	4.25	548.31	2.060016	0.000017	0.712943
P003-2	731.28	5.54	421.20	1.756314	0.000023	0.721521
P005-1	699.52	8.37	256.72	1.335597	0.000012	0.704894
P005-2	660.72	8.00	253.94	1.342687	0.000013	0.718814
P006	420.56	33.76	36.35	0.797300	0.000010	0.707996
P007-2	562.49	4.51	395.88	1.695863	0.000016	0.723276
P008	384.86	39.67	28.27	0.778773	0.000010	0.709320

Sample No.	Sm (ppm)	Nd (ppm)	$^{147}Sm/^{144}Nd$	$^{143}Nd/^{144}Nd$ [a]	±2 σ	$\varepsilon_{Nd}(0)$ [b]	$\varepsilon_{Nd}(t)$	$T_{DM\,2}$(Ma) [c]
P001	9.93	25.13	0.238885	0.512473	0.000009	−3.2	−4.1	1.316
P002	5.44	14.06	0.233799	0.512451	0.000016	−3.6	−4.4	1.348
P003-2	14.43	26.13	0.333777	0.512579	0.000015	−1.2	−4.1	1.298
P005-1	4.66	10.41	0.270508	0.512509	0.000022	−2.5	−4.1	1.303
P006	8.39	28.13	0.180321	0.512394	0.000015	−4.8	−4.4	1.303
P008	5.63	23.10	0.147399	0.512372	0.000008	−5.2	−4.1	1.287

[a] Sr and Nd isotopic ratios were corrected for mass fractionation assuming $^{88}Sr/^{86}Sr$ = 8.375209 and $^{146}Nd/^{144}Nd$ = 0.7291 following exponential functions. [b] calculated from CHUR values of $^{143}Nd/^{144}Nd$ = 0.512638 and $^{147}Sm/^{144}Nd$ = 0.1967 [40]. $\varepsilon_{Nd}(0)$ = $[(^{143}Nd/^{144}Nd)_{sample}/0.512638 - 1] \times 100{,}000$. [c] DM model age calculation assumed $^{143}Nd/^{144}Nd$ = 0.51315 and $^{147}Sm/^{144}Nd$ = 0.2137 [41,42]. $T_{DM\,2} = T_{DM\,1} - (T_{DM\,1} - t)[(f_{cc} - f_{sample})/(f_{cc} - f_{DM})]$, where f_{cc}, f_{sample}, $f_{DM} = f_{Sm/Nd}$ represent estimated mean continental crust, sample, and estimated mean depleted mantle, respectively. Calculations assume $f_{cc} = -0.4$, f_{DM} = 0.08592, and t = the emplacement age of the granite [5,11,43].

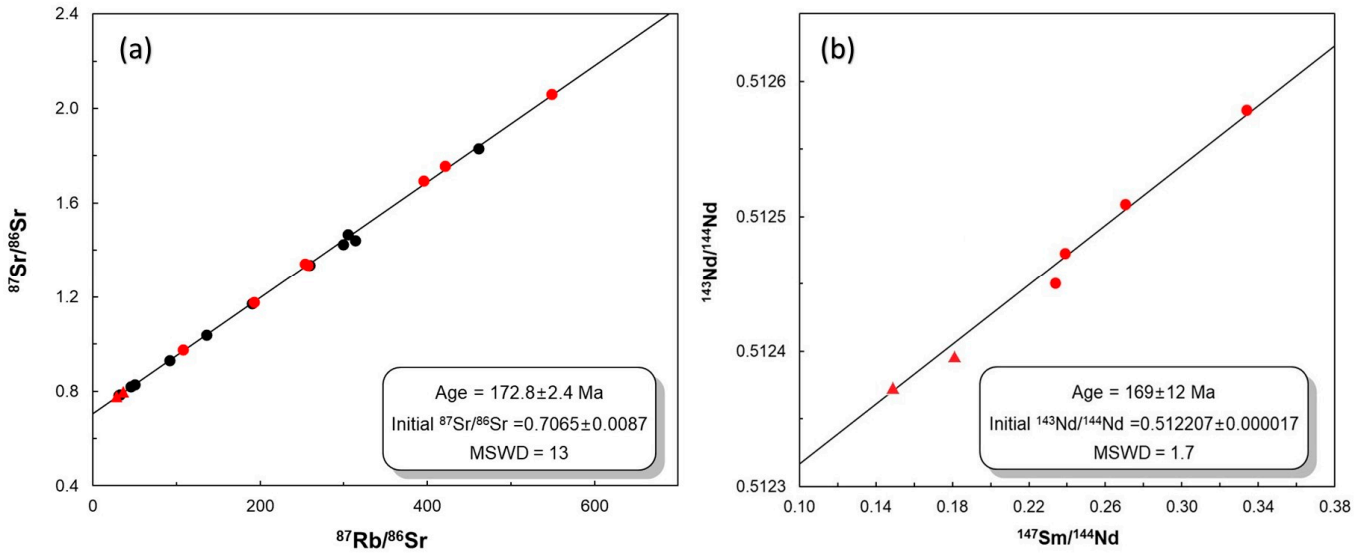


Figure 5. (**a**) Whole-rock Rb-Sr and (**b**) Sm-Nd isochrons for the Pirrit Hills granite; ● this study (B group); ▲ this study (A group); ● Millar and Pankhurst [27].

5. Discussion

5.1. Geochemical Significance of Rb-Sr and Sm-Nd Isotope Systematics and REE Tetrad Features

It is well known that both Sm and Nd are much less mobile than Rb, Sr, Th, U, and Pb whereas both Rb and Sr are relatively mobile elements, and the Rb-Sr isotopic system may readily be disturbed by the influx of a geological fluid.

In the previous report [25], Lee et al. reported the U-Pb zircon age of 164.5 ± 2.3 Ma (MSWD = 1.3), which is the average age using three zircons separated from P001, P002, and P006. This U-Pb zircon age overlaps within error with the new Rb-Sr (172.8 ± 2.4 Ma) and Sm-Nd (169 ± 12 Ma) ages in this study. Nevertheless, Rb-Sr whole rock age show slightly older age compared to Sm-Nd whole rock age and U-Pb zircon age. Sm-Nd age

also is slightly older than U-Pb zircon age. This reverse among the Rb-Sr, Sm-Nd and U-Pb zircon ages seems to suggest a disturbance of these isotopic systems. Particularly, if we consider that the U-Pb zircon age of 164.5 Ma indicates the magmatic age of the Pirrit Hills granite, we may need to re-consider the geochemical meaning of the Rb-Sr whole rock age of 172.8 ± 2.4 Ma.

Shai et al. [15] proposed that, based on Rayleigh fractionation modeling, REE tetrad effect in high-silica granite was inherited from fractional crystallization rather than formed by fluid-melt interaction. However, the authors did not mention the Sr-Nd isotope systems. Hydrothermal alterations, such as melt-fluid interactions, can lead to a transformation of the geological clock like Rb-Sr isotope system and Sm-Nd isotope system. For example, the Sm-Nd isotope system reported by Lee et al. [18] also showed a larger error range in ages (94 ± 27 Ma) than the Rb-Sr isotope system (88.1 ± 0.8 Ma), suggesting that the Sm-Nd and Rb-Sr isotopic systems might be disturbed by a geochemical reaction such as hydrothermal alteration. Nevertheless, one of the authors of this paper, S-G. Lee, argued that, based on the Sr-Nd-Ce isotope systems, the REE tetrad effect in the highly fractionated A-type granite was formed by magmatic fractionation rather than by hydrothermal alteration [17,18]. If this argument is correct, the chondrite-normalized REE pattern in Figure 4 and Rb-Sr and Sm-Nd isotope systems in Figure 5 raise an interesting question for REE geochemistry and isotope geochemistry. For example, Rb-Sr and Sm-Nd isotope systems in Figure 5 were affected by $^{87}Rb/^{86}Sr$ and $^{147}Sm/^{144}Nd$ ratios of the granites with almost no REE tetrad effect (redsolid triangles). Additionally, their Nd and Sr isotopic ratios are less radiogenic compared to those of the granite with REE tetrad effect. However, the granites with a relatively striking REE tetrad effect are more radiogenic, and they are all Sm enriched. This seems to make it difficult to say that the REE tetrad effect is entirely a product of fractional crystallization of specific minerals.

Lee et al. [25] mentioned that they discarded spot data that have U content higher than 10,000 ppm and/or have cracks/inclusions on the analysis spot area based on the method by Williams and Hergt [44]. However, White and Ireland [45] found that the relationship between apparent age and U content above 2500 ppm is not always defined, even within the same samples. It means that criteria to discard data and to apply additional correction of Lee et al. [25] may be arbitrary and inappropriate in the data manipulating procedure without an objective basis, suggesting that an emplacement age of 164.5 ± 2.3 Ma is not reliable. Particularly, apparent zircon age from three granites samples (P001, P002, P006) reported by Lee et al. [25] ranges from 150.1 Ma to 178.5 Ma. Therefore, we tried to re-interpret the U-Pb zircon age and zircon texture from the Pirrit Hill Granite in this study.

Figure 6a–f are BEC images of three zircons (P001, P002, and P006) from the Pirrit Hill granite used in Lee et al. [25]. Zircons of the Pirrit Hill granite mostly have euhedral grain shape but some are subhedral due to local leaching and resorption. Zircon grains show different internal textures under BEC images and are generally grouped into 2 types based on the difference in chemical compositions and presence or absence of inclusions and/or an inherited core. Type 1 is characterized by an oscillatory zoned core with low U concentration surrounded by rims with high U concentration, some of which have inclusion-rich bands (Figure 6a–c), while type 2 has a inclusion-rich core surrounded by an inclusion-free oscillatory zoned rim (Figure 6d–f). Zircon grains commonly have radial and/or grain boundary parallel fractures regardless of internal textures. It means that leaching of primary zircon grains and growth of secondary minerals rigorously occurred along these fractures, probably due to post-magmatic hydrothermal alteration (late-stage of magmatic event).

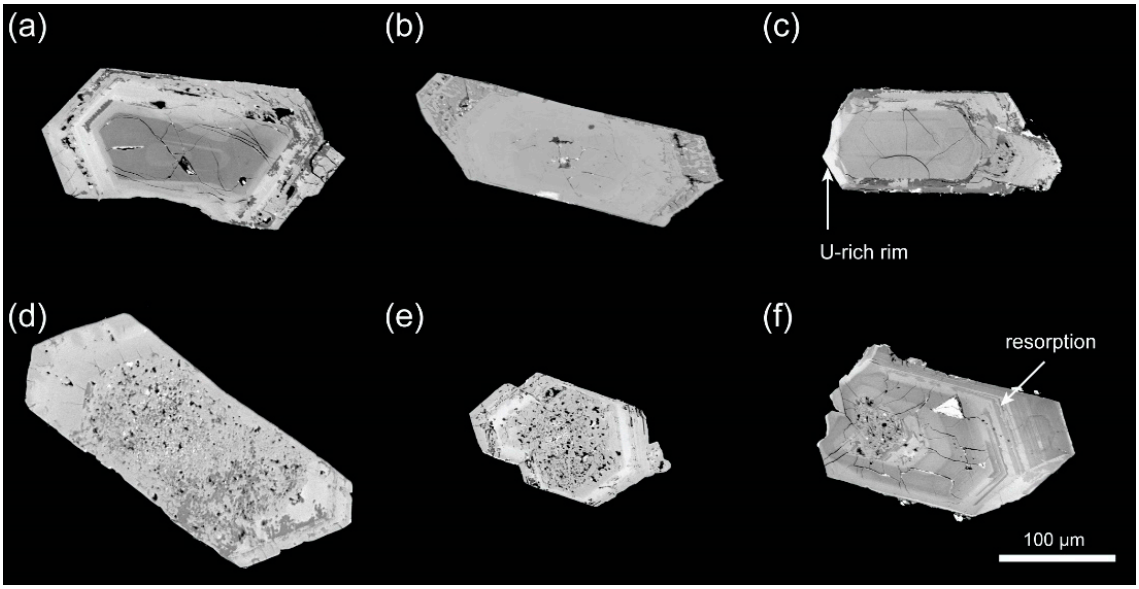


Figure 6. Representative BEC images of analyzed zircons by Lee et al. [25]. (**a**,**d**), (**b**,**e**), and (**c**,**f**) belong to samples P001, P002, and P006, respectively. Zircons separated from the three rock samples can be grouped type 1 (**a**–**c**) and type 2 (**d**–**f**) based on chemical composition and internal textures.

5.2. REE Tetrad Effects and Eu Anomalies from the Pirrit Hills Granite

Chondrite-normalized REE patterns for the Pirrit Hills granite can be divided into two groups according to Sm/Nd ratio (Figure 4). A group (Figure 4a) exhibits enriched LREE and flat HREE patterns with large negative Eu anomalies (Eu/Eu* = 0.14–0.25). B group (Figure 4b) exhibits depleted LREE and slightly enriched HREE patterns with extremely large negative Eu anomalies (Eu/Eu* = 0.01–0.09) with M-type REE tetrad effect. The degree of tetrad effect was quantified using methods described in Irber [4] and Monecke et al. [7]. B group samples with $T_1 > 0.1$ or $TE_{1,3} > 1.1$ [7] can be interpreted as showing tetrad effects. Following estimates described in Irber [4], the $TE_{1,3}$ values range from 0.96 to 1.14 with a mean value of 1.10.

Ballouard et al. [46] suggested that the Nb/Ta ratio of ~ 5 represents a threshold between a purely magmatic system (Nb/Ta) and a magmatic-hydrothermal system (Nb/Ta < 5). The Nb/Ta ratio of the granites of group A without REE tetrad effect ranges 4.26 to 20.61, whereas that of group B ranges from 1.42 to 9.01. It means that the granites in group A might have evolved under a purely magmatic system whereas the granites in group B evolved under a magmatic-hydrothermal transition system.

In Figure 7a, the relationship between Rb/Sr and SiO_2 suggest that they may have originated from different source magma. However, in Figure 7a,b, a negative correlation of the Rb/Sr vs. Sr concentration and Eu/Eu* seems to suggest feldspar-dominated fractionation from the same source magma. If this assumption is correct, Rb-Sr and Sm-Nd isotope plots in Figure 5 should be interpreted as showing that the Pirrit Hills granite was emplaced from magmatic differentiation of re-homogenized granitic magma by a purely granitic magma and hydrothermal solution under a magmatic–hydrothermal transition system. The highly fractionated Tianmenshan granites reported by Chen et al. [47] also show similar geochemical features in trace and REE geochemistry. It means that the source magma having the REE tetrad effect might be derived from fluid-melt reactions between a purely granitic magma and hydrothermal solution.

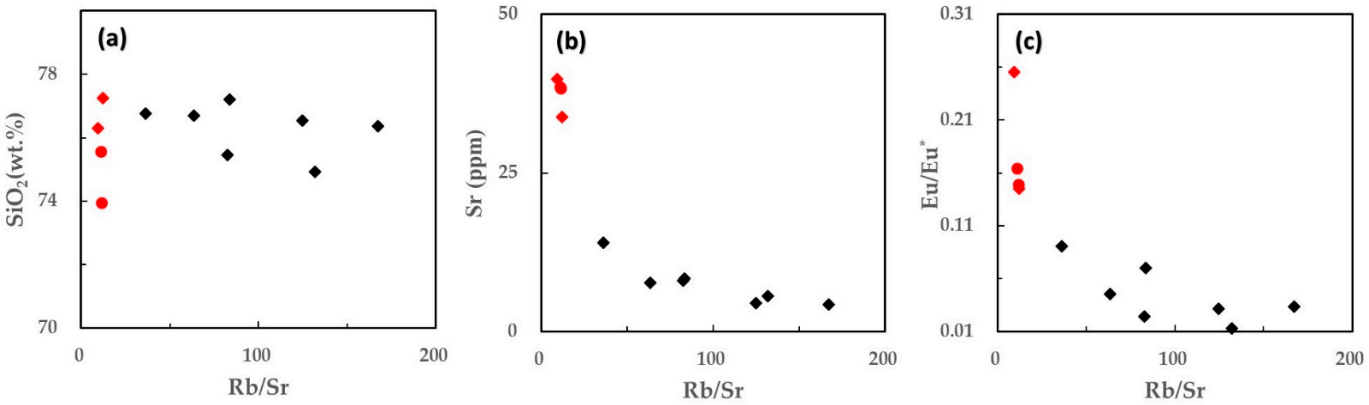


Figure 7. (**a**) SiO_2, (**b**) Sr, and (**c**) Eu/Eu* vs. Rb/Sr variation diagrams; ● A group (ICP-MS data); ♦ A group (TIMS data); ♦ B group (TIMS data).

Figure 8a is a diagram for degree of Eu anomaly (Eu/Eu*) vs. $TE_{1,3}$ values. The degree of Eu negative anomaly clearly increases in proportion to the degree of tetrad effect ($TE_{1,3}$). Lee et al. [25] suggested that, based on the depletion of the elements such as Ba, Sr, P, Zr, Eu, and Ti, the Pirrit Hills granite has undergone extensive plagioclase and K-feldspar fractionation and minor fractionation of apatite, zircon, and Fe-Ti oxides. Strontium is a compatible element in plagioclase and alkali feldspar matrices while rubidium is incompatible in plagioclase and slightly compatible to incompatible in alkali feldspar [48,49]. Fractional crystallization or partial melting effects can also appear in Rb and Sr data [49–51].

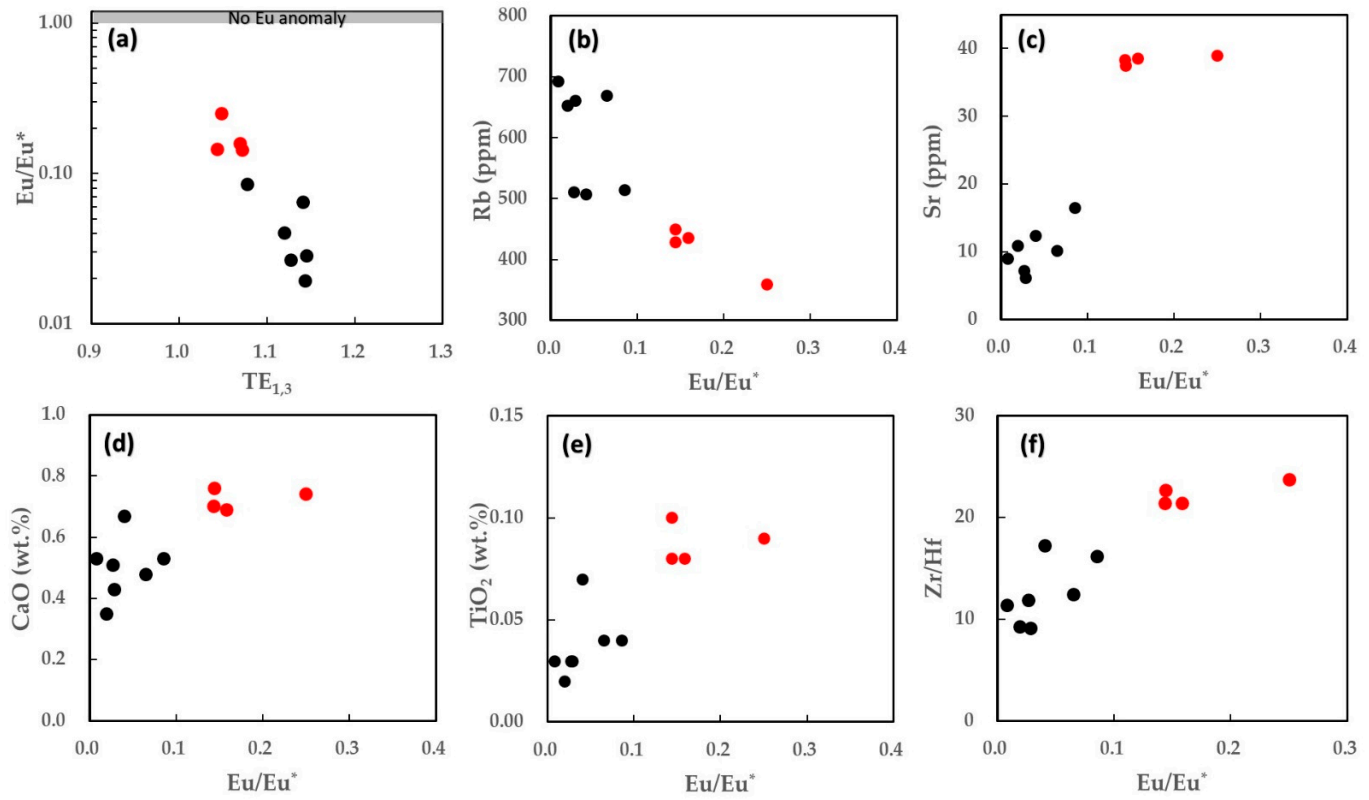


Figure 8. Eu/Eu* vs. (**a**) tetrad effects, (**b**) Rb, (**c**) Sr, (**d**) CaO, (**e**) TiO_2, and (**f**) Zr/Hf variation diagrams; ● A group; ● B group.

The Rb and Sr vs. Eu/Eu* diagram for the Pirrit Hills samples show a negative and positive relationship between these elements, suggesting that fractionation involved both alkali feldspar and plagioclase phases, respectively (Figure 8b,c). In addition, the CaO, TiO_2, and Zr/Hf ratio also reveal that they have a positive relationship with the degree of Eu anomaly (Figure 8d–f). Therefore, various geochemical characteristics related to the pronounced negative Eu anomalies, including the tetrad effect ($TE_{1,3} > 1.1$) from the Pirrit Hills granite, can be interpreted as showing that the Eu anomaly was derived from feldspar fractionation during magmatic differentiation.

However, the relationship between twin element ratios (La/Nb and Zr/Hf) and $TE_{1,3}$. (Figure 9a,b) indicates that the REE tetrad effect might be a product of a fluid-melt interaction rather than fractional crystallization. Therefore, our data seems to suggest that the Eu anomaly of the Pirrit Hills granite is likely to have occurred with the REE tetrad effect after formation of granitic magma under a magmatic-hydrothermal transition system.

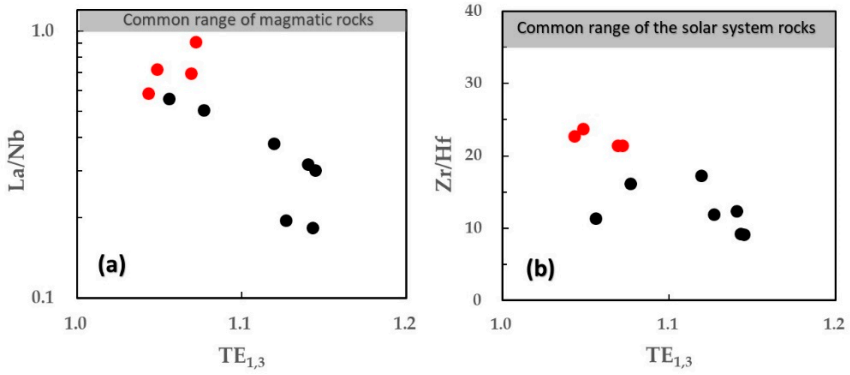


Figure 9. (**a**) La/Nb and (**b**) Zr/Hf vs. tetrad effects. Gray bands refer only to elemental ratios and not to $TE_{1,3}$ values [4]; • A group; • B group.

6. Conclusions

The Pirrit Hills granite exhibits strong REE tetrad effects and pronounced negative Eu anomalies (Eu/Eu* = 0.01~0.25). B group samples had $T_1 > 0.1$ and $TE_{1,3}$ values ranging from 0.96 to 1.14 with a mean value of 1.10. Standard geochemical ratios (Y/Ho, Zr/Hf, and Nb/Ta) indicate non-CHARAC behavior consistent with pronounced tetrad effects. Diagrams of Eu/Eu* versus other components (e.g., SiO_2, CaO, TiO_2, and Sr) or versus tetrad effect parameters ($TE_{1,3}$) indicate a close association between tetrad effects and negative Eu anomalies consistent with these geochemical features originating due to magmatic differentiation. The Rb-Sr and Sm-Nd isotope system from the Pirrit Hills granite, along with chondrite-normalized REE pattern and geochemical features of trace elements, suggest that the Pirrit Hills granite was emplaces by granitic magma produced under a magmatic-hydrothermal transition system. Therefore, the REE tetrad effect and pronounced negative Eu anomaly from the Pirrit Hills granite might be a product of the fractional crystallization of granitic magma produced under a magmatic-hydrothermal transition system.

Author Contributions: Conceptualization and methodology, S.-G.L. and H.M.L.; investigation, J.I.L. and M.J.L.; resources, J.I.L.; writing—original draft preparation, S.-G.L., H.M.L., and H.K.; writing—review and editing, S.-G.L.; funding acquisition, H.M.L. and S.-G.L. All authors have read and agreed to the published version of the manuscript.

Funding: This research was supported by the Basic Research Project of the Korea Institute of Geoscience and Mineral Resources (KIGAM) funded by the Ministry of Science and ICT (GP2020-019, H.M.L.) and the National Research Foundation of Korea (NRF) through grant no. (MSIT) (2020R1F1A1075924, NP2020-012, S.-G.L.).

Acknowledgments: We thank two anonymous reviewers for helpful and constructive reviews of the manuscript.

Conflicts of Interest: The authors declare no conflict of interest.

References

1. Masuda, A.; Kawakami, O.; Dohmoto, Y.; Takenaka, T. Lanthanide tetrad effects in nature: Two mutually opposite type W and M. *Geochem. J.* **1987**, *21*, 119–124. [CrossRef]
2. Masuda, A.; Akagi, T. Lanthanide tetrad effect observed in leucogranites from China. *Geochem. J.* **1989**, *23*, 245–253. [CrossRef]
3. Bau, M. Controls on the fractionation of isovalent trace elements in magmatic and aqueous systems: Evidence from Y/Ho, Zr/Hf, and lanthanide tetrad effect. *Contrib. Miner. Petrol.* **1996**, *123*, 323–333. [CrossRef]
4. Irber, W. The lanthanide tetrad effect and its correlation with K/Rb, Eu/Eu*, Sr/Eu, Y/Ho, and Zr/Hf of evolving peraluminous granite suites. *Geochim. Cosmochim. Acta* **1999**, *63*, 489–508. [CrossRef]
5. Jahn, B.M.; Wu, F.; Capdevila, R.; Martineau, F.; Zhao, Z.; Wang, Y. Highly evolved juvenile granites with tetrad REE patterns: The Woduhe and Baerzhe granites from the Great Zing'an mountains in NE China. *Lithos* **2001**, *59*, 171–198. [CrossRef]
6. Takahashi, Y.; Yoshida, H.; Sato, N.; Hama, K.; Yusa, Y.; Shimizu, H. W- and M-type tetrad effects in REE patterns for water-rock systems in the Tono uranium deposits, central japan. *Chem. Geol.* **2002**, *184*, 311–335. [CrossRef]
7. Monecke, T.; Kempe, U.; Monecke, J.; Sala, M.; Wolf, D. Tetrad effect in rare earth element distribution patterns: A method of quantification with application to rock and mineral samples from granite-related rare metal deposits. *Geochim. Cosmochim. Acta* **2002**, *66*, 1185–1196. [CrossRef]
8. Monecke, T.; Dulski, P.; Kempe, U. Origin of convex tetrads in rare earth element distribution patterns of hydrothermally altered siliceous igneous rocks from the Zinnwald Sn-W deposit, Germany. *Geochim. Cosmochim. Acta* **2007**, *71*, 335–353. [CrossRef]
9. Minuzzi, O.R.R.; Neto, A.C.B.; Formoso, M.L.L.; Andrade, S.; Janasi, V.A.; Flores, J.A. Rare earth element and yttrium geochemistry applied to the genetic study of cryolite ore at the Pitinga mine (Amazon, Brazil). *An. Acad. Bras. Ciênc.* **2008**, *80*, 719–733. [CrossRef]
10. Bau, M. The lanthanide tetrad effect in high evolved felsic igneous rocks—A reply to the comment by Y. pan. *Contrib. Miner. Petrol.* **1997**, *128*, 409–412. [CrossRef]
11. Wu, F.; Sun, D.; Jahn, B.; Wilde, S. A Jurassic garnet-bearing granitic pluton from NE China showing tetrad REE patterns. *J. Asian Earth Sci.* **2004**, *23*, 731–744. [CrossRef]
12. Peretyazhko, I.S.; Savina, E.A. Tetrad effects in the rare earth element patterns of granitoid rocks as an indicator of fluoride-silicate liquid immiscibility in magmatic systems. *Petrology* **2010**, *18*, 514–543. [CrossRef]
13. Monecke, T.; Kempe, U.; Trinkler, M.; Thomas, R.; Dulski, P.; Wagner, T. Unusual rare earth element fractionation in a tin-bearing magmatic-hydrothermal system. *Geology* **2011**, *39*, 295–298. [CrossRef]
14. Yurimoto, H.; Duke, E.F.; Papike, J.J.; Shearer, C.K. Are discontinuous chondrite normalized REE patterns in pegmatitic granite systems the results of monazite fractionation? *Geochim. Cosmochim. Acta* **1990**, *54*, 2141–2145. [CrossRef]
15. Shuai, X.; Li, S.-H.; Zhu, D.-C.; Wang, Q.; Zhang, L.-L.; Zhao, Z. Tetrad effect of rare earth elements caused by fractional crystallization in high-silica granites: An example from central Tibet. *Lithos* **2021**, *384*, 105968. [CrossRef]
16. Lee, S.-G.; Masuda, A.; Kim, H.S. An early Proterozoic leuco-granitic gneiss with the REE tetrad phenomenon. *Chem. Geol.* **1994**, *114*, 59–67. [CrossRef]
17. Lee, S.-G.; Asahara, Y.; Tanaka, T.; Kim, N.H.; Kim, K.-H.; Yi, K.; Masuda, A.; Song, Y.-S. La-Ce and Sm-Nd isotopic systematic of early Proterozoic leucogranite with tetrad REE pattern. *Chem. Geol.* **2010**, *276*, 360–373. [CrossRef]
18. Lee, S.-G.; Asahara, Y.; Tanaka, T.; Lee, S.R.; Lee, T. Geochemical significance of the Rb-Sr, La-Ce and Sm-Nd isotope systems in A-type rocks with REE tetrad patterns and negative Eu and Ce anomalies: The Cretaceous Muamsa and Weolaksan granites, South Korea. *Geochemistry* **2013**, *73*, 75–88. [CrossRef]
19. Philpotts, J.A.; Schnetzler, C.C. Europium anomalies and the genesis of basalt. *Chem. Geol.* **1968**, *3*, 5–13. [CrossRef]
20. Weill, D.F.; Drake, M.J. Europium Anomaly in Plagioclase Feldspar: Experimental Results and Semiquantitative Model. *Science* **1973**, *180*, 1059–1060. [CrossRef] [PubMed]
21. Fowler, A.D.; Doig, R. The significance of europium anomalies in the REE spectra of granites and pegmatites, Mont Laurier, Quebec. *Geochim. Cosmochim. Acta* **1983**, *47*, 1131–1137. [CrossRef]
22. Shearer, C.K.; Papike, J. Is plagioclase removal responsible for the negative Eu anomaly in the source regions of mare basalts? *Geochim. Cosmochim. Acta* **1989**, *53*, 3331–3336. [CrossRef]
23. Philpotts, J.A. Redox estimation from a calculation of Eu^{2+} and Eu^{3+} concentrations in natural phases. *Earth Planet. Sci. Lett.* **1970**, *9*, 257–268. [CrossRef]
24. Storey, B.C.; Hole, M.J.; Pankhurst, R.J.; Millar, I.L.; Vennum, W. Middle Jurassic within-plate granites in West Antarctica and their bearing on the break-up of Gondwanaland. *J. Geol. Soc. Lond.* **1988**, *145*, 999–1007. [CrossRef]
25. Lee, H.M.; Lee, J.I.; Lee, J.J.; Kim, J.; Choi, S.W. The A-type Pirrit Hills granite, West Antarctica: An example of magmatism associated with the break-up of the Gondwana supercontinent. *Geosci. J.* **2012**, *16*, 421–433. [CrossRef]
26. Vennum, W.R.; Storey, B.C. Petrology, geochemistry and tectonic setting of granitic rocks from the Ellsworth–Whitmore Mountains crustal block and Thiel Mountains, West Antarctica. In *Gondwana Six: Structure, Tectonics and Geophysics*; Mackenzie, G.D., Ed.; Geophysical Monograph 40; American Geophysical Union: Washington, DC, USA, 1987; pp. 139–150.

27. Millar, I.L.; Pankhurst, R.J. Rb-Sr geochronology of the region between the Antarctic Peninsula and the Transantarctic Mountains: Haag Nunataks and Mesozoic granitoids. In *Gondwana Six: Structure, Tectonics and Geophysics*; Mackenzie, G.D., Ed.; Geophysical Monograph 40; American Geophysical Union: Washington, DC, USA, 1987; pp. 151–160.
28. Pankhurst, R.J.; Storey, B.C.; Millar, I.L. Magmatism related to the break-up of Gondwana. In *Geological Evolution of Antarctica, Proceedings of the Fifth International Symposium on Antarctic Earth Sciences, Cambridge, UK, 23–28 August 1987*; Thomson, M.R.A., Crame, J.A., Thomson, J.W., Eds.; Cambridge University Press: Cambridge, UK, 1991; pp. 573–579.
29. Grunow, A.M.; Kent, D.V.; Dalziel, I.W.D. Mesozoic evolution of the West Antarctica and the Weddell Sea Basin: New palaeomagnetic constraints. *Earth Planet. Sci. Lett.* **1987**, *86*, 16–26. [CrossRef]
30. Storey, B.C.; Dalziel, I.W.D.; Garrett, S.W.; Grunow, A.M.; Pankhurst, R.J.; Vennum, W.R. West Antarctica in Gondwanaland: Crustal blocks, reconstruction and breakup processes. *Tectonophysics* **1988**, *155*, 381–390. [CrossRef]
31. Storey, B.C.; Dalziel, I.W.D. Outline of the structural and tectonic history of the Ellsworth Mountains-Thiel Mountains ridge. In *Gondwana Six: Structure, Tectonics and Geophysics*; Mackenzie, G.D., Ed.; Geophysical Monograph 40; American Geophysical Union: Washington, DC, USA, 1987; pp. 117–128.
32. Storey, B.C.; Macdonald, D.I.M. Sedimentary rocks of the Ellsworth-Thiel mountains ridge and their regional equivalents. *Br. Antarct. Surv. Bull.* **1987**, *76*, 21–50.
33. Lee, S.-G.; Kim, T.; Han, S.; Kim, H.-C.; Lee, H.-M.; Tanaka, T.; Lee, S.-R.; Lee, J.-I. Effect of zircon on rareearth element determination of granitoids by ICP-MS. *J. Petrol. Soc. Korea* **2014**, *23*, 337–349, (In Korean with English Abstract). [CrossRef]
34. Lee, S.-G.; Kim, T.; Tanaka, T.; Lee, S.-R.; Lee, J.-I. Effect on the measurement of trace element by pressure bomb and conventional teflon vial methods in the digestion technique. *J. Petrol. Soc. Korea* **2016**, *25*, 107–119, (In Korean with English Abstract). [CrossRef]
35. Kawabe, I. Tetrad effects and fine structures of REE abundance patterns of granitic and rhyolitic rocks: ICP-AES determinations of REE and Y in eight GSJ reference rocks. *Geochem. J.* **1995**, *29*, 213–230. [CrossRef]
36. Nakamura, K.; Morishita, T.; Chang, Q.; Neo, N.; Kumagai, H. Discovery of lanthanide tetrad effect in an oceanic plagiogranite from an Ocean Core Complex at the Central Indian Ridge 25° S. *Geochem. J.* **2007**, *41*, 135–140. [CrossRef]
37. McDonough, W.F.; Sun, S.-S. The composition of the Earth. *Chem. Geol.* **1995**, *120*, 223–253. [CrossRef]
38. Ludwig, K.R. *User's Manual for Isoplot 3.6: A Geochronological Toolkit for Microsoft Excel*; Berkeley Geochronology Center Special Publication No 4; Berkeley Geochronological Center: Berkeley, CA, USA, 2008.
39. Nesbitt, H.; Young, G. Early Proterozoic climates and plate motions inferred from major element chemistry of lutites. *Nature* **1982**, *299*, 715–717. [CrossRef]
40. Wasserburg, G.J.; Jacobsen, S.B.; Depaolo, D.J.; McCulloch, M.T.; Wen, T. Precise determination of Sm/Nd ratios, Sm and Nd isotopic abundances in standard solutions. *Geochim. Cosmochim. Acta* **1981**, *45*, 2311–2323. [CrossRef]
41. Depaolo, D.J. *Neodymium isotope Geochemistry: An Introduction*; Springer: New York, NY, USA, 1988; 181p.
42. Peucat, J.J.; Vidal, P.; Bernard-Griffiths, J.; Condie, K.C. Sr, Nd and Pb isotope systematics in the Archaean low- to high-grade transition zone of south India: Syn-accretion vs post-accretion granulites. *J. Geol.* **1989**, *97*, 537–550. [CrossRef]
43. Keto, L.S.; Jacobsen, S.B. Nd and Sr isotopic variations of early Paleozoic oceans. *Earth Planet. Sci. Lett.* **1987**, *84*, 27–41. [CrossRef]
44. Williams, I.S.; Hergt, J.M. U-Pb dating of Tasmanian dolerites: A cautionary tale of SHIRIMP analysis of high-U zircon. In *Beyond 2000: New Frontiers in Isotope Geoscience: Lorne, Abstract Proceedings*; Woodhead, J.D., Hergt, J.M., Noble, W.P., Eds.; Eastren Press: Lorne, Australia, 2000; pp. 185–188.
45. White, L.T.; Ireland, T.R. High-uranium matrix effect in zircon and its implications for SHRIMP U-Pb age determinations. *Chem. Geol.* **2012**, *306*, 78–91. [CrossRef]
46. Ballouard, C.; Poujol, M.; Boulvais, P.; Branquet, Y.; Tartèse, R.; Vigneresse, J.-L. Nb-Ta fractionation in peraluminous granites: A marker of the magmatic-hydrothermal transition. *Geology* **2016**, *44*, 231–234. [CrossRef]
47. Chen, Y.; Chen, B.; Duan, X.; Sun, H. Origin of highly fractionated peraluminous granites in South China: Implications for crustal anataxis and evolution. *Lithos* **2021**. [CrossRef]
48. Nash, W.P.; Crecraft, H.R. Partition coefficients for trace elements in silicic magmas. *Geochim. Cosmochim. Acta* **1985**, *49*, 2309–2322. [CrossRef]
49. Frost, D.C.; Frost, B.R.; Beard, J.S. On silica-rich granitoids and their eruptive equivalents. *Am. Min.* **2016**, *101*, 1268–1284. [CrossRef]
50. Hanson, G.N. The application of trace elements to the petrogenesis of igneous rocks of granitic composition. *Earth Planet. Sci. Lett.* **1978**, *38*, 26–43. [CrossRef]
51. Halliday, A.N.; Davidson, J.P.; Hildreth, W.; Holden, P. Modelling the petrogenesis of high Rb/Sr silicic magmas. *Chem. Geol.* **1991**, *92*, 107–114. [CrossRef]